Magnetic Resonance in Medicine 54:299–308 (2005)

Application of Model-Free Analysis in the MR Assessment of Pulmonary Perfusion Dynamics

Kai-Hsiang Chuang,[1,2] Ming-Ting Wu,[1,3*] Yi-Ru Lin,[1,2] Kai-Sheng Hsieh,[3,4] Ming-Long Wu,[2] Shang-Yueh Tsai,[2] Cheng-Wen Ko,[1,5] and Hsiao-Wen Chung[2]

Dynamic contrast-enhanced (DCE) MRI has been used to quantitatively evaluate pulmonary perfusion based on the assumption of a gamma-variate function and an arterial input function (AIF) for deconvolution. However, these assumptions may be too simplistic and may not be valid in pathological conditions, especially in patients with complex inflow patterns (such as in congenital heart disease). Exploratory data analysis methods make minimal assumptions on the data and could overcome these pitfalls. In this work, two temporal clustering methods—Kohonen clustering network (KCN) and Fuzzy C-Means (FCM)—were concatenated to identify pixel time-course patterns. The results from seven normal volunteers show that this technique is superior for discriminating vessels and compartments in the pulmonary circulation. Patient studies with five cases of acquired or congenital pulmonary perfusion disorders demonstrate that pathologies can be highlighted in a concise map that combines information of the mean transit time (MTT) and pulmonary blood volume (PBV). The method was found to provide greater insight into the perfusion dynamics that might be overlooked by current model-based analyses, and may serve as a basis for optimal hemodynamic quantitative modeling of the interrogated perfusion compartments. Magn Reson Med 54: 299–308, 2005. © 2005 Wiley-Liss, Inc.

Key words: pulmonary perfusion; dynamic contrast-enhanced MRI; data analysis; temporal clustering; pathology

Proper regulation of pulmonary perfusion and ventilation is required for efficient gas exchange. Therefore, it is essential to accurately estimate pulmonary perfusion to assess the pathophysiology of the lung. In current clinical practice, pulmonary perfusion is evaluated with the use of nucleotide scintigraphic methods. However, these techniques are limited by poor spatial resolution and artifacts introduced by long imaging times (1). Magnetic resonance imaging (MRI) has been demonstrated to be a promising tool for evaluating brain perfusion with a spatial resolution of less than 1.5 mm and temporal resolution of about 1 s using Gd-DTPA as a contrast agent (2). When the same strategy is extended to image pulmonary perfusion, the poor magnetic field homogeneity caused by the complex air–tissue interfaces in the lung reduces the T_2^* of the lung tissue to only a few milliseconds. The resulting low signal-to-noise ratio (SNR) limits the application of MRI in the lungs. Recent developments in short-TE imaging sequences have overcome the T_2^* decay and made it feasible to assess pulmonary perfusion by dynamic contrast-enhanced (DCE) MRI, as used in brain perfusion studies (1,3–7).

Assuming that the contrast agent is a nondiffusible, intravascular tracer, quantitative indices, such as the relative pulmonary blood volume (PBV), relative mean transit time (MTT), and relative pulmonary blood flow (PBF), can be derived from the time courses of signal intensity (SI) in DCE-MRI (1,8,9). To eliminate the SI change from recirculation of the tracer, the time course is fitted to an assumed bolus-shaped function (typically a gamma-variate function) before the calculation is performed. Summary parameters, such as time-to-peak and gamma-fitting parameters, can be obtained as well (10). Furthermore, to achieve the absolute quantification of PBV, PBF, and MTT, a suitable arterial input function (AIF) is required to deconvolve the delayed and dispersed agent concentrations if the tracer transit function is linear.

However, in contrast to the brain, which has the blood–brain barrier, the contrast agent can diffuse to the surrounding tissues in the lungs, thus violating the assumption of an intravascular tracer. Complicated tracer kinetics in pulmonary parenchyma also invalidate the assumptions of a gamma-variate function and linear system in three situations: 1) when the lung parenchyma has altered permeability, such as in interstitial pneumonitis or pulmonary edema; 2) when the pulmonary artery has altered intrapulmonary circulation, such as in pulmonary artery hypertension or thromboembolism; and 3) when the pulmonary artery has an altered inflow pattern from the heart or an altered outflow pattern back to the heart, as in congenital heart disease. All of these situations could greatly alter the inflow/outflow patterns of pulmonary circulation and render the derived quantification inaccurate, thus hindering the assessment of pathology.

Since quantitation of PBF and PBV is challenging due to the use of extravascular tracers, and changes in permeability and flow during disease states, an alternative method that can provide objective and concise differentiation of the hemodynamics in the pulmonary circulation is in great demand. Exploratory data analysis methods such as temporal clustering (11,12) and independent component anal-

[1]Department of Radiology, Kaohsiung Veterans General Hospital, Kaohsiung, Taiwan, R.O.C.

[2]Department of Electrical Engineering, National Taiwan University, Taipei, Taiwan, R.O.C.

[3]Faculty of Medicine, School of Medicine, National Yang Ming University, Taipei, Taiwan, R.O.C.

[4]Department of Pediatrics, Kaohsiung Veterans General Hospital, Kaohsiung, Taiwan, R.O.C.

[5]Department of Computer Science and Engineering, National Sun Yat-sen University, Kaohsiung, Taiwan, R.O.C.

Grant sponsor: Kaohsiung Veterans General Hospital Research Program; Grant numbers: VGHKS94-040; VGHKS94G-23; Grant sponsor: National Science Council; Grant number: NSC-92-2314-b-037-099.

Presented at the 11th Annual Meeting of ISMRM, Toronto, Canada, 2003.

*Correspondence to: Ming-Ting Wu, M.D., Chief, Section of Thoracic Imaging, Department of Radiology, Kaohsiung Veterans General Hospital, 386 Tachung 1st Rd., Kaohsiung 811, Taiwan, R.O.C. E-mail: mingting.wu@isca.vghks.gov.tw or wumt@seed.net.tw

Received 1 June 2004; revised 6 January 2005; accepted 7 February 2005.

DOI 10.1002/mrm.20551

Published online in Wiley InterScience (www.interscience.wiley.com).

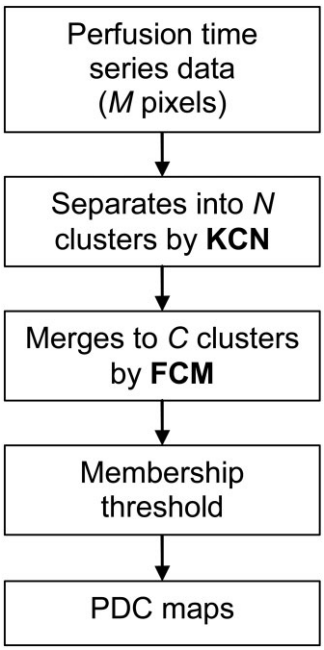

FIG. 1. Flowchart of the KCN-FCM analysis.

ysis (13) make only minimal assumptions regarding the signal dynamics, and hence could eliminate the errors from inaccurate modeling. Recently these methods were applied to extract the AIF (14) and reduce large-vessel effects in the perfusion map (15). In this paper we propose to combine two temporal clustering methods—Kohonen clustering network (KCN) and Fuzzy C-Means (FCM) (12)—to identify components with different tracer dynamics in the heart and lungs (i.e., the perfusion dynamic component (PDC) map). Since the interrogated components include the beating heart and central vasculature, we adopted an ECG-gated, interleaving, notched saturation fast gradient-echo sequence that was recently developed for cardiac perfusion imaging (16) to minimize physiological motion and enhance contrast while maintaining sufficient slice coverage. A comparison of the current results and the model-based PBV and MTT findings shows that this analysis method can provide more insights into the precise tracer kinetics in normal and pathological conditions, and may serve as a basis for optimal perfusion quantification.

MATERIAL AND METHODS

Theory

Temporal clustering methods are used to group pixels with similar SI variations into a cluster, and thus provide a way to distinguish regions with analogous perfusion dynamics. Here we introduce a two-stage method that concatenates two different temporal clustering methods: KCN and FCM. The idea is to perform overclustering of the perfusion time series data by a fast clustering method (KCN) and then merge redundant clusters by FCM. Figure 1 shows the processing flowchart of the KCN-FCM analysis.

KCN is an unsupervised neural network that is based on Kohonen's self-organizing map (SOM) model (17). By regarding a pixel time-course as a vector, SOM classifies M input vectors into N ($N < M$) cluster features according to their Euclidean distance. Since the original SOM algorithm is a non-optimization process, it is sensitive to initial conditions, noise, and so forth. We thus adopted the modification proposed by Pal et al. (18) to minimize a weighted sum of square error:

$$\Gamma = \frac{\sum_{k=1}^{M}\sum_{i=1}^{N} g_{ki}\|\mathbf{I}_k - \mathbf{V}_i\|^2}{\mathbf{M}} \quad [1]$$

$$g_{ki} = \begin{cases} 1 & \text{if } i = n_m \\ \dfrac{1}{\sum_{j=1}^{N} \|\mathbf{I}_k - \mathbf{V}_j\|^2}, & \text{otherwise;} \end{cases}$$

where $\mathbf{I}_k$ is the kth input vector, $\mathbf{V}_i$ is the ith cluster feature, and n_m is the best matching cluster of $\mathbf{I}_k$.

The basic procedures of KCN are summarized below:

1. Randomly initialize N feature vectors.
2. Compare each input vector with the N features to find the most similar feature, i.e., the *winner*. Then assign this input to be a member of the winning cluster.
3. Modify the *winner* feature to make it resemble the input vector. In other words, the *winner* learns the characteristics of the input vector. In addition, the modification is applied to other cluster features—not just the *winner*—to stabilize the algorithm.
4. Iterate steps 2 and 3 until the changes are less than a specified threshold for all cluster features. These cluster features will then converge to the most representative features of all input vectors.

Because of its simple structure, KCN is very efficient in terms of processing speed and memory usage. However, KCN has to designate each input to only one cluster, even when this input is similar to more than two clusters, and this "hard" partitioning property makes it difficult to classify ambiguous features. To overcome this limitation but retain the advantages of KCN, the data are first overclassified by KCN and then the identified cluster features are merged by the second clustering method, FCM. Unlike KCN, FCM does not determine to which cluster one input vector belongs (19). On the contrary, it calculates a membership function that describes the probability that one input vector belongs to each output cluster. If one input vector matches one of the C cluster features perfectly, the probability of belonging to that cluster should be one, and the probability of belonging to other clusters should be zero. If there is no perfectly matching cluster, the membership $\mu_{m,n}$ between the mth input and the nth cluster is determined by the following equation:

$$\mu_{m,n} = \frac{1}{\sum_{k=1}^{C} \left(\dfrac{\|\mathbf{I}_m - \mathbf{V}_n\|}{\|\mathbf{I}_m - \mathbf{V}_k\|} \right)^{2/p-1}}, \quad [2]$$

where $\boldsymbol{I}_m$ is the mth input vector, $\boldsymbol{V}_n$ is the nth cluster feature, and p (>1) is the fuzzy factor. The basic procedures of FCM are summarized below:

1. Randomly initialize N feature vectors.
2. Compare each input vector with the N features and calculate its membership.
3. Modify all cluster features by the membership-weighted sum of the input vectors to make them learn the characteristics of the input vectors.
4. Iterate steps 2 and 3 until the membership function converges. Then use a membership threshold to determine to which cluster an input belongs.

MRI Experiment

Data Acquisitions

Two groups of subjects were enrolled in the present study. In the first group (seven healthy male volunteers, 20–27 old) we developed the methodology and evaluated normal pulmonary perfusion physiology. In the second group, which consisted of five patients, we examined our method under pathophysiological circumstances. The second group included three adult patients (one with lung cancer, one with Swyer-James syndrome, and one with single lung transplantation with postoperative pulmonary artery stenosis) and two pediatric patients (one (2 years 4 months old) with Tetralogy of Fallot, and one (8 months old) with complex congenital heart disease with major aortopulmonary collateral circulation). Informed consent was obtained from the subjects or their parents before scanning was performed. The experiment protocol was approved by the Institutional Review Board of Kaohsiung Veterans General Hospital.

Images were acquired by a GE Signa CV*i* 1.5T imager (GE Healthcare, Milwaukee, WI, USA). An ECG-gated, magnetization-prepared, 2D segmented gradient-echo echo-planar sequence with interleaved notched saturation pulses was used (16). To minimize susceptibility effects, short echo times (TEs) and echo train lengths were achieved by acquiring four echoes per segment. The interleaved notched saturation scheme utilized a band-stop RF profile at the beginning of the slice acquisition to presaturate the magnetization in the next slice to be acquired. This technique effectively provided a longer recovery time for stronger T_1 weighting than ordinary magnetization-prepared fast gradient-echo methods, while it also allowed more slices to be acquired within one trigger interval. The parameters were dependent on heart rates. Typically, TR/TE/TI = 6.6/1.1/181 ms, and flip angle (FA) = 20° were used. After three baseline frames, paramagnetic contrast medium (Gd-DTPA, Magnavist, Schering; dosage = 0.05 mM/kg) was rapidly injected with a saline flush. In the adults, the injection was performed by a power injector at a rate of 3.0 mL/s. Hand injection was performed as fast as possible (about 1–1.5 mL/s) in the children. There were two scanning protocols: 1) TR = 1 R-R interval, 2–3 slices, slice thickness = 6 mm to center on the pulmonary hila; and 2) TR = 2 R-R intervals, 6–8 slices, slice thickness = 15 mm to cover the entire lung parenchyma. Thirty to 60 frames were acquired in each protocol. The adult subjects were asked to hold their breath during the perfusion scan, and the children breathed freely under sedation. Four healthy subjects underwent both protocols at an interval of 2 hr. The FOV was 480 mm and the data matrix of 128 × 128 was interpolated to 256 × 256 by zero padding. 3D MRA was also performed on the patients for a detailed morphological evaluation of the pulmonary vasculature.

Data Processing

Perfusion dynamic component (PDC) map obtained by the KCN-FCM method. KCN and FCM analyses were performed with custom-written software (Functional MRI Analysis and Clustering Tools (FACT); free download at http://mr.ee.ntu.edu.tw/~khchuang/fact.html), running under Linux (Red Hat, NC, USA). Before clustering was performed, uninteresting pixels were discarded and the SIs were normalized. To remove the pixels we used two thresholds: one was a background threshold to remove pixels outside the body, and the other was a signal variation threshold, which was the average of the standard deviation (SD) divided by the mean in the background, to remove pixels that did not possess significant enhancement, such as in muscle and fat. The SI normalization was done by dividing the time-course signal by its median.

After preprocessing was performed, the data were first clustered into 50 features by KCN and then grouped into 10–18 patterns by FCM. KCN was initialized by randomly selecting input vectors, and FCM was initialized by randomly generating unit vectors. In addition, the identified KCN features were normalized as unit vectors before processing by FCM was performed. The similarity measure used in FCM was the Euclidian distance. The fuzzy factor was 1.3, and the membership threshold was 0.8. The processing time for one slice, which consisted of 20000 to 25000 input pixels, was about 30–40 s on a PC with a Pentium 4 1.8G Hz CPU (Intel, CA, USA). Cluster waveforms showing perfusion-related signal changes were selected and displayed in colors according to the time-to-peak. Then pixels belonging to the selected clusters were mapped by the corresponding colors to create a PDC map.

MTT and PBV maps obtained by the gamma-fitting method. Quantitative perfusion analysis, using the model proposed by Hatabu et al. (8), was performed independently by an observer blinded to the results of KCN-FCM. The program was developed locally with Matlab 6.5 (MathWorks, Natick, MA, USA). The images were first smoothed spatially by averaging the signal intensities within a 3 × 3 window. The signal time course was then fitted by a gamma-variate function to calculate the relative MTT and normalized by an AIF to derive the relative PBV (9). The beginning point of the gamma fitting was chosen as the point before 10% of the maximum enhancement was exceeded. The ending point of the fitting was chosen to be the sixth time point after the maximum enhancement. To avoid fitting pixels outside the lung, we used two thresholds: one to discard pixels without prominent signal changes, and one to remove pixels with too strong of an enhancement, as in the liver, by discarding any pixel enhanced more than 150% from baseline. Finally, MTT and PBV maps were generated with pseudo-color to maximize the contrast in the lung.

RESULTS

Healthy Subjects

The ECG-gated interleaved notched segmented echo-planar imaging (EPI) successfully eliminated cardiac motion

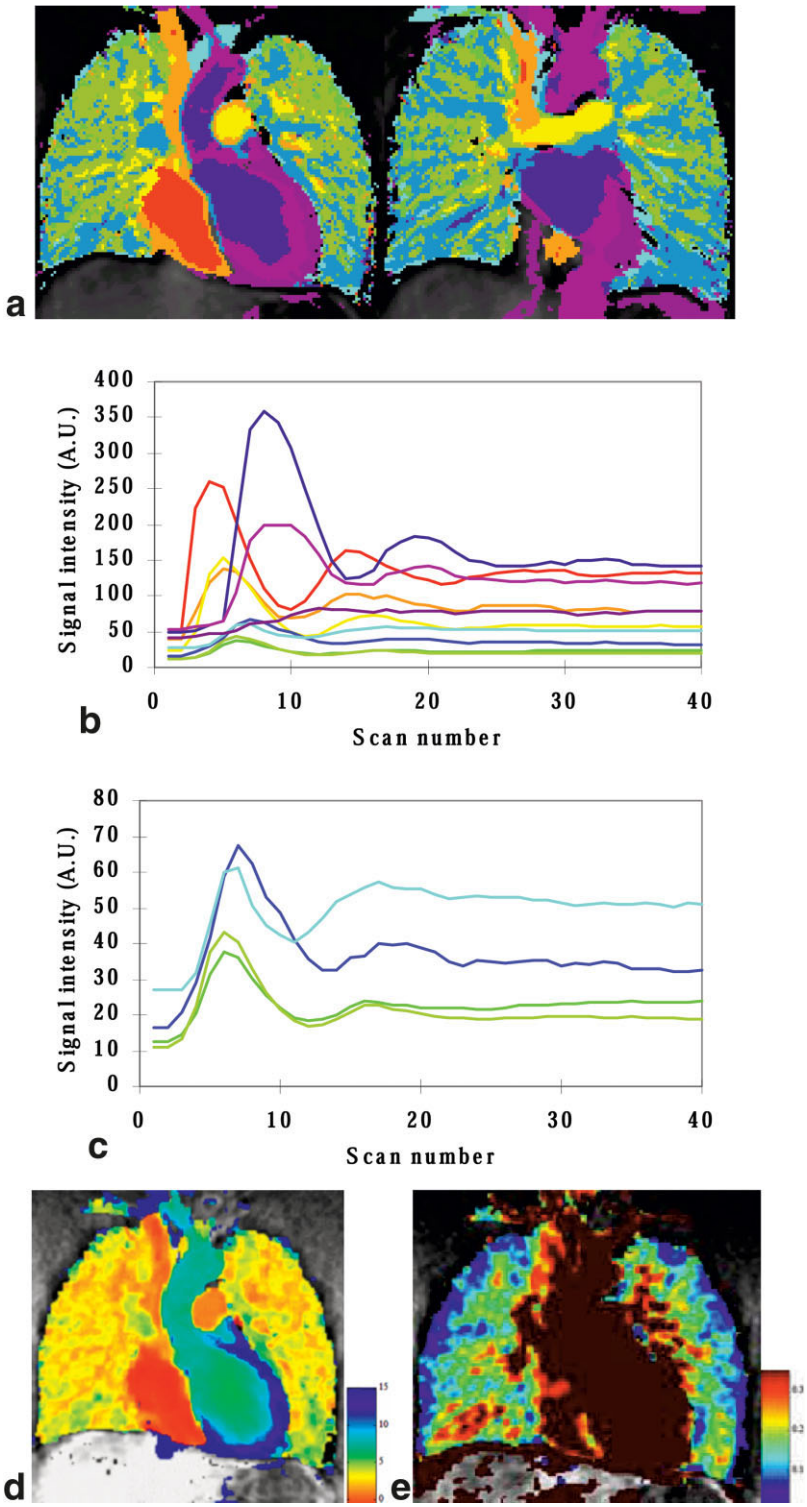

FIG. 2. **a:** PDC maps of two adjacent slices from a healthy subject. The perfusion components are pseudo-colorized from red to blue according to the perfusion consequence as follows: superior vena cava (orange), right ventricle (red), pulmonary arteries (yellow), lung parenchyma (green, olive green, and cyan), pulmonary vein and left atrium (steel blue and blue), left ventricle and aorta (blue), and inferior vena cava (magenta). **b:** The averaged SI time courses of the major components of the first slice in part a. The time courses in the lung parenchyma are magnified in **c**. **d:** The MTT map of the first slice in part a with pseudo-color in the unit of scan number. Most components in the PDC map correspond to regions with different MTTs. **e:** The relative PBV map of the first slice in part a with the unit normalized to an AIF. This confirms that in PDC maps the component in the central lung parenchyma (steel blue) corresponds to higher blood volume, and the component in the peripheral lung (cyan) corresponds to lower blood volume. Therefore, PDC maps present the combined information of MTT and PBV. It also shows that the lower part of the lung has higher but slower perfusion (steel blue) than the upper part (olive green). [Color figure can be viewed in the online issue, which is available at www.interscience.wiley.com.]

and provided high contrast-to-noise ratio (CNR) images in all normal volunteers. Figure 2a shows the PDC maps of two adjacent slices from a healthy volunteer analyzed by KCN-FCM. The spatially averaged SI time courses of the clusters in the first slice are shown in Fig. 2b, and those in the lung parenchyma are magnified in Fig. 2c. Major components in the cardiovascular system are clearly differentiated and pseudo-colorized from red to blue in the order of circulation consequence as follows: superior vena cava (orange), right atrium and right ventricle (red), pulmonary artery trunk and bilateral main pulmonary arteries (yellow), segmental pulmonary arteries and lung parenchyma (green, olive green, and cyan), pulmonary veins and left atrium (steel blue and blue), left ventricle and aorta (blue), inferior vena cava and myocardium (magenta), and spleen (purple). Figure 2d and e show the MTT and PBV maps,

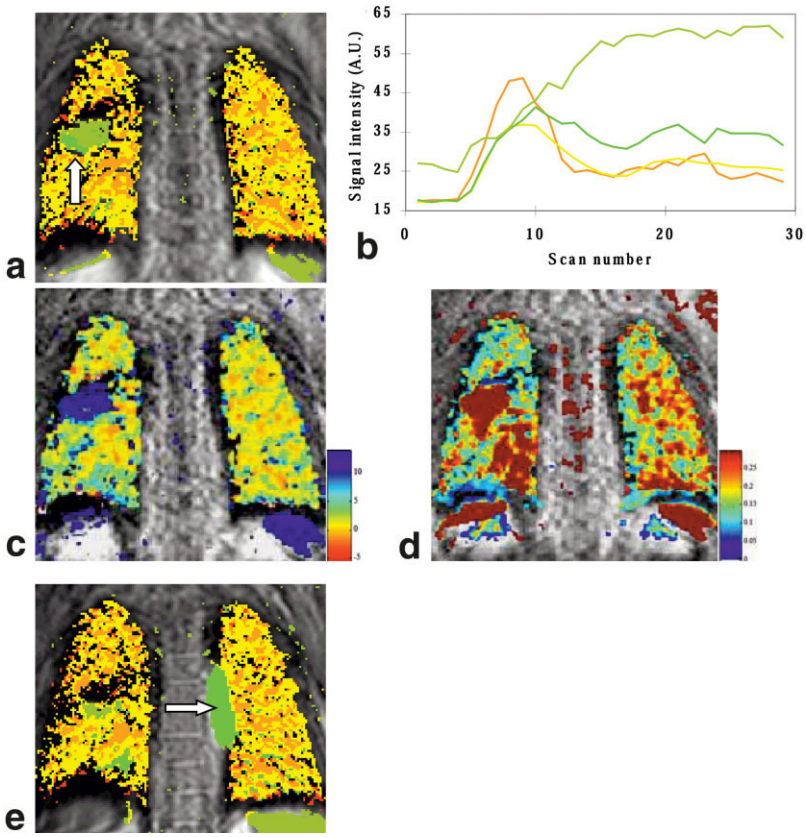

FIG. 3. A 65-year-old male with lung cancer in the right upper lobe. **a:** The PDC map clearly marked the tumor (arrow) as dark green mixed with small parts of light green clusters (arrow). **b:** The averaged SI time course of each cluster. The (**c**) MTT and (**d**) PBV maps confirm that the lung tumor has slow and large flows, respectively; however, the boundary of the tumor is ill-defined in the PBV map. With the advantage of multislice analysis, we found that the light green cluster of the tumor had the same peak time as the descending aorta (arrow) in another slice (**e**). This finding suggests that the tumor receives its blood supply from a branch of the aorta (i.e., the bronchial artery). It should be noted that the patient failed to sustain the breath-hold well, which resulted in a sudden signal change on the 23rd scan. [Color figure can be viewed in the online issue, which is available at www.interscience.wiley.com.]

respectively, of the first slice in Fig. 2a. In the PBV map, the variation in the mediastinum could not be differentiated because pseudo-color was used to maximize contrast in the lungs. When the three maps were compared, most clusters in the PDC map (Fig. 2a) corresponded to regions with different MTTs. However, the superior vena cava, RV, and pulmonary arteries were better separated by the PDC map than by the MTT because these regions have high blood volume. This indicates that the PDC map also contains information on the PBV. In addition, regions with different perfusion in the lungs were also differentiated by KCN-FCM (in green and blue colors). The upper part of the lung showed more olive green areas than the lower part, while the lower part of the lung showed more steel blue areas than the upper part (Fig. 2a). From the averaged SI time courses in these clusters (Fig. 2c), it can be seen that the steel blue cluster is enhanced later and higher than the olive green cluster, indicating that the lower lung has a longer MTT and higher PBV. This upper–lower lobar gradient, which is in accord with normal perfusion physiology (9), was better shown by the PDC map than by the PBV map, and was more prominent in the posterior slice (the second slice) than in the anterior slice (the first slice).

We found that in the healthy subjects, four major segments of the hemodynamic consequent phases could be consistently divided:

1. Right-atrium → right ventricle → pulmonary trunk → bilateral main pulmonary arteries.
2. Lung parenchyma.
3. Pulmonary vein → left atrium.
4. Left ventricle → aorta.

Generally, about five (median = 5, range = 4–7) clusters (including pulmonary arteries, veins, and parenchyma) could be discriminated in the lung parenchyma, and about six (median = 6, range = 5–8) clusters (including atriums, ventricles, arteries, veins, and myocardium) could be differentiated in the heart. A comparison of scans with interframe intervals of 2 R-R and 1 R-R revealed that the identified clusters in similar slice positions were very close, but overall, more clusters could be identified using 2 R-R. Although 1 R-R provided better temporal resolution, 2 R-R appeared to be sufficient to separate the major compartments while allowing for more slice numbers (e.g., seven vs. three slices) to cover broader areas of the lungs and the cardiac system. Furthermore, the PDC maps of 2 R-R had better quality because the SNR of the 2 R-R data was higher due to the thicker slices and more time for longitudinal relaxation. Based on the above advantages, we used only the 2 R-R technique in the patient studies.

Patients

Acquired Pulmonary Perfusion Disorders

Figure 3 shows the results from a patient with lung cancer. The PDC (Fig. 3a) and MTT (Fig. 3c) maps both clearly identify the tumor in the middle of the right lung. Although the PBV map (Fig. 3d) also shows the abnormality, the boundary can not be differentiated from the nearby high blood volume regions. In addition, the PDC map indicates that there are two components in the tumor, one of which is synchronized with that of the descending aorta (Fig. 3e). This indicates that the tumor receives a blood

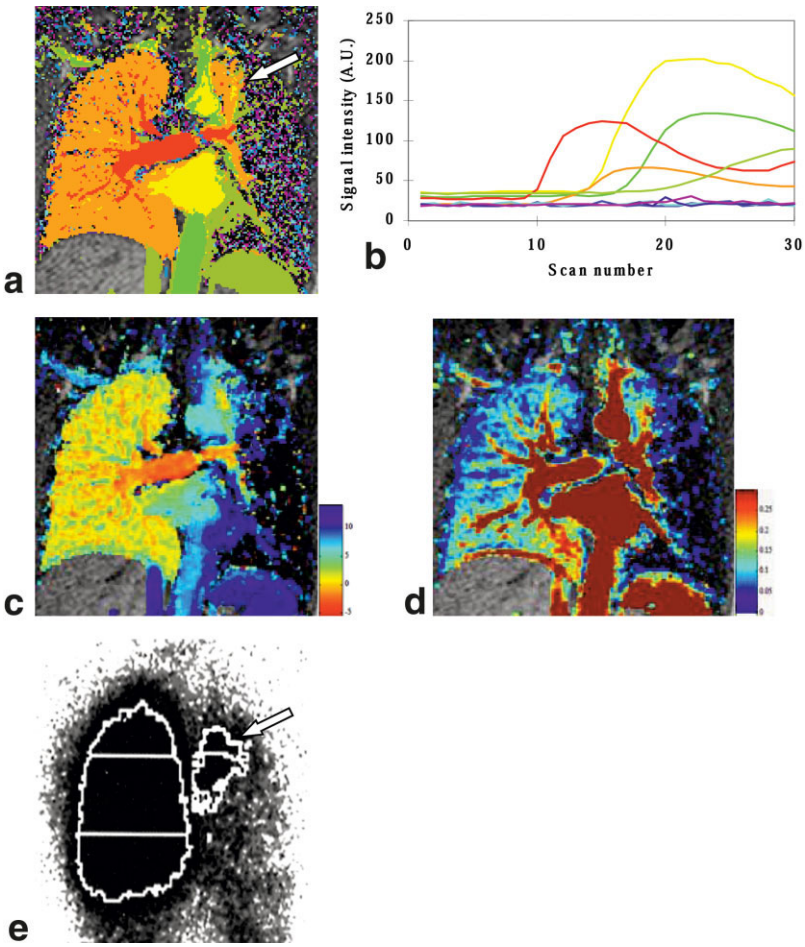

FIG. 4. A 23-year-old male with acquired obliteration of the unilateral pulmonary arteries and a small airway due to childhood bronchiolitis (Swyer-James syndrome). The (**a**) PDC map and (**b**) averaged SI time curve of each cluster are shown. Note that the left lower lobe has almost no perfusion, and the width of the signal enhancement in the right lung is much wider than that in normal cases. Compared to the (**c**) MTT and (**d**) PBV maps, the PDC and PBV maps better identify the small portion of normal left upper lung (arrow). **e:** Tc99M-MAA perfusion scintigraphy with exaggerated gain confirms the presence of the left apical lung (arrow). [Color figure can be viewed in the online issue, which is available at www.interscience.wiley.com.]

supply from a branch of the aorta (i.e., the bronchial artery). Since malignant lung tumors get most of their blood supply from the aorta (in contrast to benign tumors, which get their blood from the pulmonary artery), this finding helped us to characterize the tumor.

Figure 4 shows a representative slice from a patient with Swyer-James syndrome, a disease that involves acquired obliteration of the unilateral pulmonary arteries due to bronchiolitis during childhood. The PDC map (Fig. 4a) shows scarce SI in the left lung (Fig. 4b), indicating severe perfusion deficit in the left lung. The combination of the MTT (Fig. 4c) and PBV (Fig. 4d) maps largely agrees with this result. However, only the PDC and PBV maps identify the small portion of normal left upper lung (arrow in Fig. 4a). The status of the left apical lung was confirmed by Tc99M-MAA perfusion scintigraphy (Fig. 4e). Identification of the small normal apical lung is important because it may expand to compensate for lung function after the diseased lower lung is resected.

Congenital Pulmonary Perfusion Disorders

Figure 5 shows the results from a 3-year-old patient with Tetralogy of Fallot after total correction with residual left peripheral pulmonary stenosis. While the PDC (Fig. 5a) and MTT (Fig. 5c) maps showed differences between the left and right lungs, the PBV map (Fig. 5d) appeared similar in the bilateral lungs. This incorrect measurement was due to poor model fitting of the perfusion dynamics. As indicated by the delayed SI curve in the left lung (the cyan line in Fig. 5b), there may have been some overlap with the second-pass transit. Thus, the PBV may have been overestimated, which led to an appearance that was indistinguishable from the SI curve in the normal lung parenchyma (the green line in Fig. 5b). If this is the case, a careful examination of both the MTT and PBV maps will be needed. Furthermore, the PDC map clearly shows branches of the pulmonary artery in the right lung (Fig. 5a, orange color, arrow), whereas they are absent in the left lung. This was confirmed by conventional invasive angiography (Fig. 5e, arrow). This finding is important because it suggests that the deficient and delayed perfusion of the left lung was due to peripheral stenosis of the left pulmonary artery after a surgical procedure. The SI curves of some clusters in the lungs also showed a large fluctuation from the respiratory motion. This was because the sedated children could not hold their breath during the scan. The KCN-FCM analysis identified this signal change and worked well even in this condition. This robustness is important for analyzing pediatric data.

Figure 6 shows a 1-year-old patient with pulmonary atresia and a major aortopulmonary collateral artery. The KCN-FCM analysis (Fig. 6a) was better at discriminating perfusion deficiency in the left apical lung than the MTT-PBV method (Fig. 6c and d). In addition, KCN-FCM solely

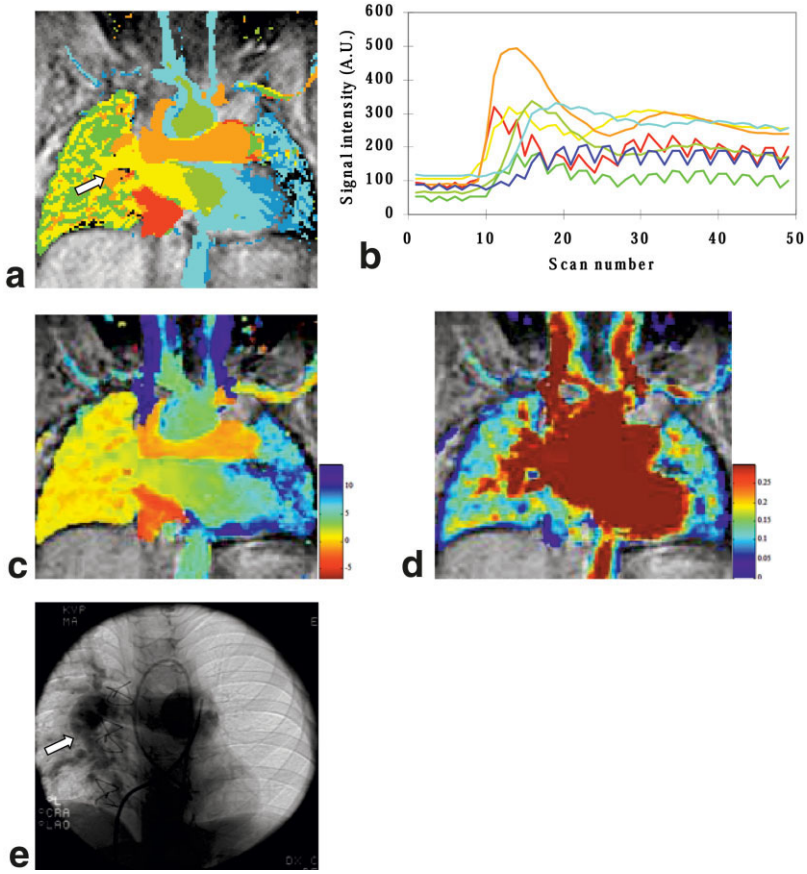

FIG. 5. A 3-year-old patient with Tetralogy of Fallot received surgical total correction for severe peripheral stenosis of the left main pulmonary artery. The (**a**) PDC map and (**b**) averaged SI time curve in each cluster, and the (**c**) MTT and (**d**) PBV maps are shown. Both the PDC and MTT maps (but not the PBV map) show distinct perfusion patterns in the left lung vs. the right lung. In addition, the PDC map clearly shows the branches of the pulmonary artery in the right lung (orange color, arrow), while they are absent in the left lung. This finding was confirmed by conventional invasive angiography (**e**, arrow). Note that even with jittered patterns due to regular respiratory motion in free breathing, the KCN-FCM analysis still worked well. [Color figure can be viewed in the online issue, which is available at www.interscience.wiley.com.]

demonstrated a distinct perfusion pattern of the aorta in the right upper lung (Fig. 6a, red cluster), indicating a possible connection with the descending aorta. This was confirmed by MRA (Fig. 6e), which showed a large collateral artery (arrow) from the descending aorta to the right upper lung. Identification of the aortic collateral artery is important because it must be ligated after total correction of Tetralogy of Fallot is performed.

DISCUSSION

We have demonstrated the feasibility of a model-free method, KCN-FCM, for analyzing pulmonary perfusion MRI. This method distinguished regions with different perfusion kinetics without assuming forms of the signal enhancement. In normal volunteers, vessels and compartments at different time phases of the pulmonary circulation were differentiated. This ability to segment anatomical-functional complexes facilitated subsequent studies on perfusion in different functional regions, such as the pulmonary arteries/veins, lung parenchyma, and left/right heart. Several kinds of pathological conditions were evaluated. The boundaries of the abnormalities were clearly delineated, and the actual tracer kinetics in interrogated compartments (normal or abnormal) were easily visualized and compared. In addition, since this method is also sensitive to other kinds of signal fluctuations, it could be used to identify artifacts, such as motion artifacts (Fig. 3b and 5b), to evaluate the quality of the data.

Current quantitative perfusion analyses rely on a presumed perfusion kinetic function to obtain quantitative parameters for diagnosis. They also include operator-dependent procedures, such as selecting the time interval for function fitting, which are difficult to perform in complicated pathological situations. Although the proposed method did not provide quantitative indices, it presented an objective, concise, hemodynamic segmentation on one single map. The cluster waveform obtained from this analysis provided an easy way to visualize the major tracer kinetics in the lungs. In some of the patients (e.g., Figs. 4b and 6b) the dynamics of the contrast agent were quite different from those of the normal condition, even in regions without lesions. Thus, pathological conditions would not be fully described by the analysis based on an assumed model derived from healthy subjects, and the estimation of the actual MTT, PBV, and PBF would be biased. The normal and pathological phenomena identified by this model-free analysis method not only helped us to understand the actual kinetics that would be overlooked by model-based methods, they also assisted in the creation and testing of new models.

Ideally, model-free analyses should differentiate areas with distinctive signal enhancements, which represent the distinction between MTT, PBV, and/or PBF. The KCN-FCM results showed that most of the clusters were close to regions with different MTTs. Only a small portion of the clusters were similar to regions with different PBVs. This was mainly due to the SI normalization used in both

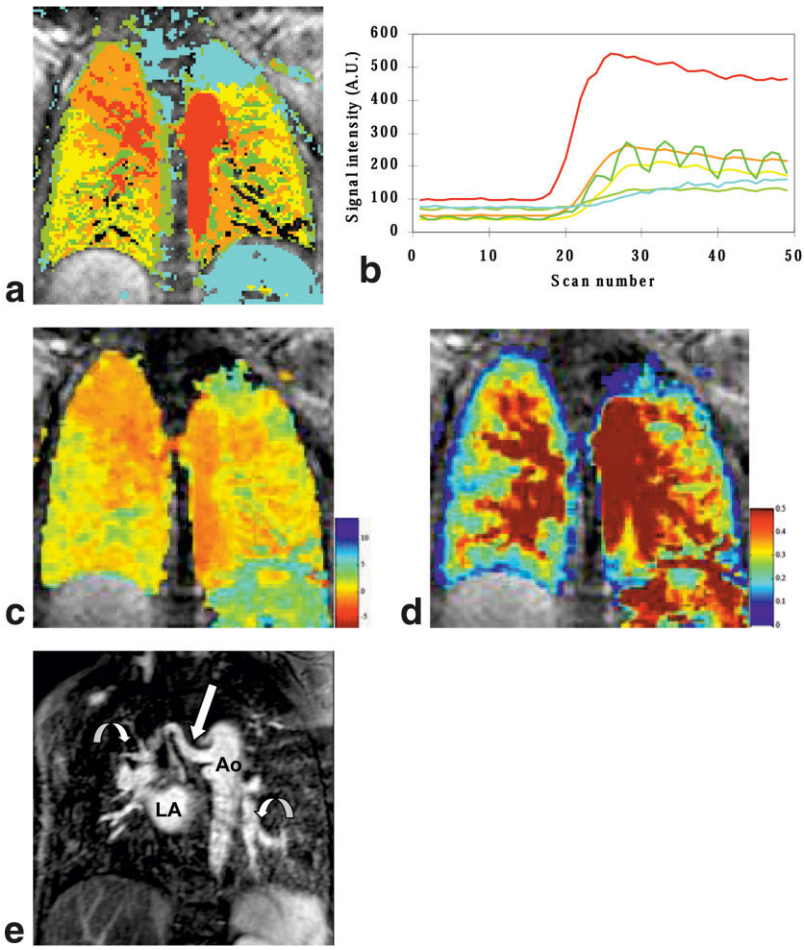

FIG. 6. A 1-year-old patient with Tetralogy of Fallot and major aortopulmonary collateral arteries. The (**a**) PDC map and (**b**) averaged SI time curve in each cluster, and the (**c**) MTT and (**d**) PBV maps are shown. KCN-FCM analysis discriminated perfusion deficiency in the left apical lung better than the MTT-PBV method. In addition, the PDC map solely demonstrated a distinct perfusion pattern of the aorta in the right upper lung (red), which suggests that the right upper lung received blood supply from the aorta instead of the pulmonary artery. This was confirmed by MRA (**e**), which showed a large aortopulmonary collateral artery (arrow) from the descending aorta to the right upper lung. LA, left atrium of the heart; Ao, descending aorta; curved arrows, pulmonary arteries. [Color figure can be viewed in the online issue, which is available at www.interscience.wiley.com.]

algorithms. Intensity normalization was necessary to make the algorithms classify based on the shape of the waveform but not the amplitude. Suitable normalization was also required so that the algorithms would converge to a minimum more easily. After intensity normalization was performed, the differences in the amplitudes, which were related to the integral of the signal change, were diminished. Thus, only large differences in the PBV could be discriminated. We tested several normalization strategies (results not shown) and found that we could achieve better differentiation of most structures by dividing by the median of the time course in KCN.

The proposed method concatenates two different kinds of clustering algorithms. If either algorithm is used alone, it is difficult to achieve both sufficient separation of features and efficient processing. This two-stage clustering approach takes advantage of the fast processing property of KCN and the ambiguous feature-separating capability of FCM to obtain a better balance between effectiveness and efficiency. An additional advantage is that a more detailed analysis of a region, such as the lungs, can be attained by displaying the KCN clusters included in this area. Interrogated analysis on the lung parenchyma per se can also be achieved by removing the clusters corresponding to major vessels and the heart.

Of all of the parameters in the KCN and FCM algorithms, the cluster number was the one that affected the analysis result the most. Finding the optimum cluster number is one of the most difficult issues in cluster analysis. Classifying data for too many clusters makes analysis and interpretation tiresome, while obtaining too few clusters results in mixed features. Since it was difficult to estimate the exact number of different patterns in the data, we let KCN overclassify the data, and used FCM to group similar clusters together. In our study we found that it was sufficient to set the cluster number of KCN at 50. Using too large a cluster number only reduced the efficiency of the processing. The optimum cluster number for FCM was variable and depended on the complexity of the patterns identified by KCN. Hence, it was adjusted case by case. Algorithms that could automatically split or combine clusters based on some separation-compactness indices may eliminate the problem of choosing the optimal cluster number (20).

Since the SNR of the lungs was still lower than that of the muscles, liver, or heart, we had to exclude uninteresting regions to focus on identifying the pattern of interest. Otherwise, the patterns in the lungs would be misclassified and produce misleading results. This would be an issue in cases of disease because the data quality is usually inferior to that of normal volunteers. We adopted several strategies to eliminate the pixels with little or too much signal enhancement. Nonetheless, some background regions and tissues were retained. Using a manually selected region of interest or a mask of the lungs to restrict the

analysis region could reduce misclassification and improve the separation of patterns with lesser disparity.

For a finer description of the tracer kinetics and better differentiation of the signal enhancement of less significant differences, it would be advisable to use an interframe interval of 1 R-R because it could provide more temporal information. However, the slice number, i.e., the spatial coverage, would largely be limited. This would hinder the observation of the full extent of the lesion sites and the relations of tracer kinetics between different regions. A comparison of the 2 R-R and the 1 R-R results in the normal volunteers indicated that the major clusters were similar, since 2 R-R was enough to record the dynamics of the perfusion enhancement. Furthermore, with higher SNR of the 2 R-R data, the KCN-FCM analysis results had better quality.

To minimize physiological motion and enhance T_1 contrast, we innovatively applied ECG-gated, interleaved notch-saturation segmented gradient-echo EPI to study the contrast-enhanced pulmonary perfusion. Since a TE of 1.1 ms and an image acquisition time of 200 ms were achieved with four echoes per segment, the SNR in the lung was adequate without noticeable ghosting from the heart. For example, the typical SNR in the lung parenchyma of a normal volunteer without enhancement was at least 7–8, and the peak percentage enhancement of the lung parenchyma was about 150–250%. Although the use of the notched saturation pulse may raise concerns about the signal in regions with fast flow, in our experience we did not observe any distortion of the input function. The magnetization-prepared fast gradient-echo sequences, which are commonly used in DCE-MRI of pulmonary perfusion [3,5], required long recovery times to achieve sufficient T_1 contrast. However, this limited the number of slices that could be acquired within one trigger interval. With a band-stop saturation pulse applied in advance to saturate the next slice to be acquired, this new method provided a recovery time that was long enough without sacrificing slice coverage. In our experiments, three slices could be acquired with high CNR within the 1 R-R interval. Furthermore, compared to fast 3D MRA, which is usually used to examine the lung, this ECG-gated fast imaging showed only a slight misregistration due to respiratory motion, rather than the blurred 3D data of 2-s temporal resolution obtained by MRA. This feature is especially important when the method is applied to children.

With ECG gating, respiratory motion became the remaining major source of signal fluctuation. Signal variation caused by respiratory motion was observed in some patients due to their inability to hold their breath well. Our results showed that KCN-FCM analysis was still able to distinguish major clusters in the presence of this kind of fluctuation. The robustness with respect to motion was important when the method was applied to pediatric imaging. Since this kind of motion usually occurred in the later scans in adults, we could reduce this artifact by discarding all frames after the motion became substantial. Although this strategy improved the analysis results in our testing (results not shown), it sometimes lost information that arose late in the time course. Furthermore, this strategy would be impractical for children because when they are sedated, they are unable to hold their breath throughout the entire scanning session. For better application in children, some methods to reduce signal fluctuations from respiratory motion could be used. Since this fluctuation increases the jittering of the SI time course, one could use a window function to smooth the signal time course. Image registration algorithms that consider the deformation of the moving lungs would be a more suitable approach to eliminate the respiratory motion (21).

In future studies, we will utilize the structural-functional information obtained from the KCN-FCM analysis to improve the quantification of pulmonary perfusion. Since the progression of the tracer kinetics in major structures of the pulmonary circulation is clearly identified, models that are more comprehensive can be created and tested. The tissue perfusion could be modeled by a two-compartment model that considers Gd-DTPA as a partially diffusible agent that moves between the tissue and the capillary bed. The modeling could then be tested using the arterial input and venous output functions identified by the KCN-FCM analysis.

CONCLUSIONS

We have shown the potential of a temporal clustering method, KCN-FCM, for analyzing pulmonary perfusion MRI. In addition to visualizing the dynamics in different regions of the cardiac and pulmonary vessels and parenchyma, the time domain information provided by this method could elucidate the actual kinetics that would be overlooked by a conventional model. With this tool, the AIF could be obtained more easily, and models could be optimized to precisely quantify pulmonary perfusion.

ACKNOWLEDGMENTS

The authors would like to thank Ms. Cindy Yang for English editing.

REFERENCES

1. Uematsu H, Levin DL, Hatabu H. Quantification of pulmonary perfusion with MR imaging: recent advances. Eur J Radiol 2001;37:155–163.
2. Rosen BR, Belliveau JW, Vevea JM, Brady TJ. Perfusion imaging with NMR contrast agents. Magn Reson Med 1990;14:249–265.
3. Hatabu H, Gaa J, Kim D, Li W, Prasad PV, Edelman RR. Pulmonary perfusion: qualitative assessment with dynamic contrast-enhanced MRI using ultra-short TE and inversion recovery turbo FLASH. Magn Reson Med 1996;36:503–508.
4. Kauczor HU, Kreitner KF. Contrast-enhanced MRI of the lung. Eur J Radiol 2000;34:196–207.
5. Howarth NR, Beziat C, Berthezõne Y. Evolution of pulmonary perfusion defects demonstrated with contrast-enhanced dynamic MR perfusion imaging. Eur Radiol 1999;9:1574–1576.
6. Haraldseth O, Amundsen T, Rinck PA. Contrast-enhanced pulmonary MR imaging. MAGMA 1999;8:146–153.
7. Fratz S, Hess J, Schwaiger M, Martinoff S, Stern HC. More accurate quantification of pulmonary blood flow by magnetic resonance imaging than by lung perfusion scintigraphy in patients with fontan circulation. Circulation 2002;106:1510–1513.
8. Hatabu H, Tadamura E, Levin DL, Chen Q, Li W, Kim D, Prasad PV, Edelman RR. Quantitative assessment of pulmonary perfusion with dynamic contrast-enhanced MRI. Magn Reson Med 1999;42:1033–1038.
9. Levin DL, Chen Q, Zhang M, Edelman RR, Hatabu H. Evaluation of regional pulmonary perfusion using ultrafast magnetic resonance imaging. Magn Reson Med 2001;46:166–171.

10. Thomas DL, Lythgoe MF, Pell GS, Calamante F, Ordidge RJ. The measurement of diffusion and perfusion in biological systems using magnetic resonance imaging. Phys Med Biol 2000;45:R97–R138.
11. Scarth G, McIntyre M, Wowk B, Somorjai RL. Detection novelty in functional images using fuzzy clustering. In: Proceedings of the 3rd Annual Meeting of ISMRM, Nice, France, 1995. p 238.
12. Chuang KH, Chiu MJ, Lin CC, Chen JH. Model-free functional MRI analysis using Kohonen clustering neural network and Fuzzy C-Means. IEEE Trans Med Imaging 1999;18:1117–1128.
13. McKeown MJ, Makeig S, Brown GG, Jung TP, Kindermann SS, Bell AJ, Sejnowski TJ. Analysis of fMRI data by blind separation into independent spatial components. Hum Brain Mapp 1998;6:160–188.
14. Murase K, Kikuchi K, Miki H, Shimizu T, Ikezoe J. Determination of arterial input function using fuzzy clustering for quantification of cerebral blood flow with dynamic susceptibility contrast-enhanced MR imaging. J Magn Reson Imaging 2001;13:797–806.
15. Carroll TJ, Haughton VM, Rowley HA, Cordes D. Confounding effect of large vessels on MR perfusion images analyzed with independent component analysis. Am J Neuroradiol 2002;23:1007–1012.
16. Slavin GS, Wolff SD, Gupta SN, Foo TKF. First-pass myocardial perfusion MR imaging with interleaved notched saturation: feasibility study. Radiology 2001;219:258–263.
17. Kohonen T. Self-organizing maps. New York: Springer-Verlag; 1995.
18. Pal NR, Bezdek JC, Tsao ECK. Generalized clustering networks and Kohonen's self-organizing scheme. IEEE Trans Neural Networks 1993; 14:549–556.
19. Bezdek JC. Pattern recognition with fuzzy objective function algorithms. New York: Plenum; 1981.
20. Baune A, Sommer FT, Erb M, Wildgruber D, Kardatzki B, Palm G, Grodd W. Dynamical cluster analysis of cortical fMRI activation. Neuroimage 1999;9:477–489.
21. Torheim G, Amundsen T, Rinck PA, Haraldseth O, Sebastiani G. Analysis of contrast-enhanced dynamic MR images of the lung. J Magn Reson Imaging 2001;13:577–587.